Radiotherapy and Oncology 121 (2016) 276–280

Contents lists available at ScienceDirect

Radiotherapy and Oncology

journal homepage: www.thegreenjournal.com

Abdominal organ motion

An MRI-based mid-ventilation approach for radiotherapy of the liver

Tessa N. van de Lindt [a], Gerald Schubert [b], Uulke A. van der Heide [a], Jan-Jakob Sonke [a,*]

[a] Department of Radiation Oncology, The Netherlands Cancer Institute, Amsterdam, The Netherlands; [b] MR-Therapy, Philips, Vantaa, Finland

ARTICLE INFO

Article history:
Received 27 June 2016
Received in revised form 30 September 2016
Accepted 23 October 2016
Available online 5 November 2016

Keywords:
Respiratory motion
Mid-ventilation
MRI
Liver
MR-linac

ABSTRACT

MRI is increasingly being used in radiotherapy of the liver. The purpose of this study was to develop and validate a strategy to acquire MR images for treatment planning and image guidance in the presence of respiratory motion.

By interleaving two navigator triggered MRI sequences, a fast but low-resolution image in mid-ventilation (midV) and a high-resolution image in exhale were acquired efficiently. Deformable registration was applied to map the exhale image to the midV anatomy. Cine-MRI scans were acquired for motion quantification.

The method was validated with a motion phantom, 10 volunteers and 1 patient with a liver tumor. The time-weighted mean position of a local structure in a cine-scan was defined as the midV-position ground truth and used to determine the accuracy of the midV-triggering method. Deformable registration accuracy was validated using the SIFT algorithm.

Acquisition time of the midV/exhale-scan was 3-5 min. The accuracy of the midV-position was $\leqslant 0.5 \pm 0.5$ mm for phantom motion and $\leqslant 0.9 \pm 1.2$ mm for the volunteers. Mean residuals after deformable registration were $\leqslant 0.2 \pm 1.8$ mm. The accuracy and reproducibility of the method are within inter- and intra-fraction liver position variability (Case et al., 2009) and could in the future be incorporated in a conventional liver radiotherapy or MR-linac workflow.

In radiotherapy, computed tomography (CT) and cone-beam CT (CBCT) scans are the current clinical standard for treatment planning and position verification. However, abdominal lesions are often not clearly visible on these images because of the limited soft-tissue contrast that (CB)CT provides. Moreover, respiratory motion in the upper-abdomen challenges accurate imaging and dose delivery. Therefore, treatment of tumors in areas such as the liver requires the placement of fiducial markers or relatively large safety margins. Because of the superior soft-tissue contrast that MRI provides, there is an increasing interest in using MRI for treatment planning and image guidance. With an integrated MRI scanner and linear accelerator (MR-linac), it will even become possible to visualize abdominal lesions on the treatment machine. This could potentially lead to more accurate dose delivery facilitating margin reduction or dose escalation. Therefore, new MRI-based strategies for radiotherapy of moving targets are required.

There are various approaches to account for respiratory motion in radiotherapy. Gating and tracking are potentially accurate methods, but require real-time tumor localization and linac response [2,3]. Motion encompassing techniques such as the internal-target-volume method (ITV) or strategies based on irradiation of the time-weighted mean position of the tumor only affect the treatment preparation phase and are therefore relatively easy to use clinically [4]. The anatomy of the patient closest to the time-weighted mean position of the tumor is called the mid-ventilation (midV) anatomy [5]. By treating the patient in midV, systematic errors are reduced. As 3D motion of the tumor is incorporated in the planning-target-volume (PTV) margin, the midV approach results in a significantly smaller PTV than the ITV method [4].

Typically, the midV anatomy and tumor motion are derived from 4D-CT [5]. Current 4D-MRI techniques, however, have extensive acquisition times and/or insufficient image quality [6–9]. In this study, a method to efficiently acquire a high quality MRI in midV and quantify respiratory induced motion from additionally acquired MRI scans, for treatment planning and image guidance of liver radiotherapy, was developed and evaluated.

Materials and methods

In a typical respiratory motion pattern (Fig. 1), the time spent in inhalation is short compared to exhalation. In mid-ventilation, the velocity of the liver is high and images are most susceptible to motion artifacts. Therefore, two navigator triggered imaging sequences were interleaved [9]: (1) In midV a fast but

* Corresponding author.
E-mail address: j.sonke@nki.nl (J.-J. Sonke).

http://dx.doi.org/10.1016/j.radonc.2016.10.020
0167-8140/

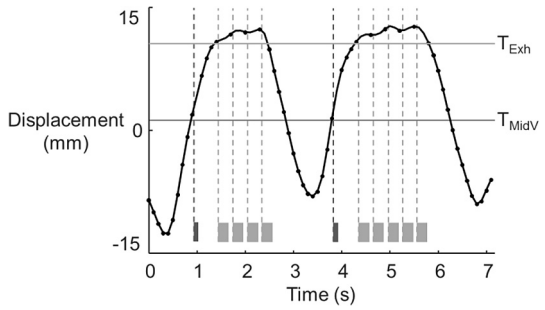

Fig. 1. Acquisition scheme. Navigator signal with exhale and midV rising trigger levels. The small blocks represent the short acquisition time in midV and the large blocks the longer multiple acquisitions in exhale.

low-resolution image ($MidV_{LR}$) was acquired to minimize motion artifacts and facilitate an accurate midV-position and (2) a high-resolution image was acquired in exhale (Exh_{HR}) to exploit the prolonged time spent in this position. Then, deformable image registration was applied to deform the Exh_{HR} image to the midV anatomy to obtain a high-resolution image in midV ($MidV_{HR}$). Additionally, a sagittal and coronal cine-MRI were acquired for motion quantification.

The method was validated with an MR-compatible motion phantom. To determine if the method is also accurate and reproducible in human subjects, it was tested in ten healthy volunteers. Additionally, one patient with liver metastasis was included following our institutional guidelines.

Acquisition and post-processing

All measurements were performed on a 1.5T whole body MR system (Achieva, Philips Healthcare, Best, The Netherlands). Two navigator triggered imaging sequences (Table 1) were interleaved [9] with a midV and an exhale trigger level (T_{MidV} and T_{Exh}). In a 30 s navigator preparation phase prior to the scan phase, T_{MidV} was defined as the average navigator position corrected for the slice acquisition time and T_{Exh} as 90% of the range of the navigator signal. For every respiratory cycle, when the navigator exceeds the upslope T_{MidV}, one axial slice of a low-resolution ($2 \times 2 \times 5mm^3$) image was acquired. Slices of a high-resolution ($1.2 \times 1.2 \times 5\ mm^3$) image were subsequently acquired as long as the navigator signal $>T_{Exh}$ (Fig. 1). SENSE was increased for the midV-scan to decrease slice acquisition time (Table 1). Voxel-size and NSA were chosen such, that SNR of both scans were approximately the same. Since for $MidV_{LR}$ only one slice per respiratory cycle was acquired and in the prolonged exhale time multiple slices, predicted total scan time of both scans was similar, meaning two scans could be acquired in the time of one. Actual total scan time is dependent on the patient's respiratory pattern.

Deformable registration of Exh_{HR} to $MidV_{LR}$ was performed using ADMIRE 1.12 (Elekta, Stockholm, Sweden) within ~17 s on an Intel Xeon CPU (2.4 GHz) system with a NVIDIA Tesla K20 GPU (2496 cores – 5 GB RAM). A deformable block-matching method with normalized-sum-of-squared-differences (NSSD) was applied in order to get a robust initial alignment. Then, a dense non-linear image transformation was computed to further refine the result and to align image details, using the local-cross-correla tion-coefficient (LCC) [10].

For 3D motion quantification, a 2D sagittal and coronal cine-MRI (Table 1) were acquired subsequently at 2 frames per second for approximately 1 min. Cranio-Caudal (CC) and anterior-posterior (AP) motion were quantified from the sagittal and the left–right (LR) motion from the coronal cine. 2D local rigid image registration with mutual information was applied on the upper part of the liver from all timeframes to an arbitrary cine reference frame, using in-house developed software. The motion amplitude was defined as the average peak-to-peak amplitude over all breathing cycles in the cine-MRI.

Phantom experiments

Phantom experiments were performed on an MR-compatible motion phantom prototype (Modus Medical Devices Inc., Canada). It is designed to move a cylindrical insert, containing a spherical compartment that mimics a tumor, in CC-direction within a body shaped oval. The compartments were filled with different concentrations of $MnCl_2$ to obtain sufficient contrast. Phantom motion was calibrated with 4D-CBCT prior to the MRI experiments.

Six waveforms based on the Lujan motion model [11] were used. Symmetrical waveforms and waveforms shaped more similar to a real respiratory signal with extended exhale phase, with varying peak-to-peak amplitudes and periods (Table 2). For every motion pattern, an interleaved midV/exhale-scan (with the navigator positioned on the cylinder boundary) and two orthogonal cine-scans centered in the tumor compartment were acquired. The cine quantified motion amplitude was compared to the phantom motion. The accuracy of the triggered midV-position was determined by comparing the position of the tumor compartment in the midV-scan with the mean position in the cine-MRI, by local rigid registration. To establish the reproducibility of the midV-triggering, the experiment was repeated 5 times with symmetric waveform B and asymmetric waveform E (Table 2). The variation in deviation from the cine-based midV-position was then investigated.

Volunteer experiments

Ten healthy volunteers were scanned according to the protocol in Fig. 2. The navigator was positioned on top of the liver to capture diaphragmatic motion. Exh_{HR} were deformed to the $MidV_{LR}$ scans

Table 1
Scan parameters for $MidV_{LR}$, Exh_{HR}, sagittal and coronal cine MRI.

Scan parameters	$MidV_{LR}$	Exh_{HR}	Sagittal cine	Coronal cine
Scan	Single-shot TSE	Single-shot TSE	Balanced FFE	Balanced FFE
Voxel size	$2 \times 2 \times 5\ mm^3$	$1.2 \times 1.2 \times 5\ mm^3$	$1.5 \times 1.5 \times 7\ mm^3$	$1.5 \times 1.5 \times 7\ mm^3$
Axial FOV	$375 \times 300\ mm^2$	$375 \times 300\ mm^2$	$320 \times 270\ mm^2$	$350 \times 360\ mm^2$
Slices	30	30	1	1
TR	270 ms	467 ms	2.8 ms	2.6 ms
TE	65 ms	65 ms	1.4 ms	1.3 ms
SENSE	2.5	2	-	-
NSA	1	3	1	1
Slice acquisition time	176 ms	352 ms	494 ms	427 ms

SENSE = sensitivity encoding (for scan time reduction), NSA = number of signal averages (for intensity increase)